# PTYCHNET : CNN BASED FOURIER PTYCHOGRAPHY

*Armin Kappeler, Sushobhan Ghosh, Jason Holloway, Oliver Cossairt, Aggelos Katsaggelos*

Department of Electrical Engineering and Computer Science,
Northwestern University,
Evanston, IL 60208, USA

**ABSTRACT**

Fourier ptychography is an imaging technique that overcomes the diffraction limit of conventional cameras with applications in microscopy and long range imaging. Diffraction blur causes resolution loss in both cases. In Fourier Ptychography, a coherent light source illuminates an object, which is then imaged from multiple viewpoints. The reconstruction of the object from these set of recordings can be obtained by an iterative phase retrieval algorithm. However, the retrieval process is slow and does not work well under certain conditions. In this paper, we propose a new reconstruction algorithm that is based on convolutional neural networks and demonstrate its advantages in terms of speed and performance.

***Index Terms—*** Fourier Ptychography, Convolutional Neural Network, CNN

## 1. INTRODUCTION

Imaging using traditional optical systems is constrained by the space-bandwidth product (SBP) [1], which describes the trade-off between high resolution and large field of view. Fourier ptychography (FP) is a coherent imaging technique which aims to overcome the SBP limitation by capturing a sequence of SBP limited images and computationally combining them to recover a high resolution, large FOV image and thus overcoming the SBP barrier. Fourier ptychography has been applied to wide field, high resolution microscopy [2], quantitative phase imaging [3], adaptive fourier ptychography imaging [4], long distance, sub diffraction imaging [5] and other applications. In fourier ptychography, a high resolution image is recovered from a set of frequency limited low resolution images of an object illuminated with coherent light source. To achieve this, an iterative phase retrieval algorithm [6] recovers the phase information that is lost in the incoherent imaging process. A detailed overview of different phase reconstruction techniques can be found in [7, 8].

Iterative phase retrieval algorithms performs well if the set of low resolution images have overlapping frequency bands in the fourier domain, but the reconstruction quality quickly degrades as the overlap between the Fourier patches decreases [9]. The requirement of overlap between neighboring patches requires sequential scanning to obtain all the low resolution images and hence, a major barrier to single shot ptychography [10]. Reducing or eliminating the overlap-requirement would lead to a much faster aquisition time. In this paper, we foucs on the algorithm for retrieving the high resolution image. In place of a phase retrieval algorithm, we propose a Convolutional Neural Network (CNN) based solution (PtychNet), that directly restores the image in the spatial domain without explicitly recovering the phase information. CNNs have been proven to be very effective for image classification [11–13], and have become increasingly popular with other image processing tasks such as super-resolution [14–16], image segmentation [17], etc.

We show that PtychNet obtains better reconstruction results in considerably less time if the low resolution images have no overlapping frequency bands. When the low-resolution images contain overlapping support in the frequency domain, we can use PtychNet to significantly reduce the computation time of an iterative phase retrieval algorithm.

The remainder of the paper is organised as follows. In Section 2 we briefly introduce Fourier Ptychography, in Section 3 we explain our proposed framework PtychNet. Sections 4 contains our results and experimental evaluation and Section 5 concludes the paper.

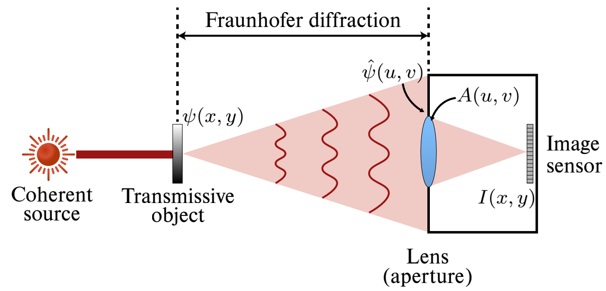


**Fig. 1**: Example setup for Fourier Ptychography (FP). Coherent light diffracts through a translucent medium into the far-field. A lens samples a portion of the Fourier domain which is recorded as intensity images at the sensor. See Section 2.1 for details.

## 2. FOURIER PTYCHOGRAPHY

### 2.1. Image Formation Model

Consider the generalized imaging setup shown in Figure 1. A monochromatic source with wavelength $\lambda$ illuminates a transparent object. Let the 2D complex field that emanates from the object be denoted as $\psi(x, y)$. If a camera is placed in the far-field and satisfies the Fraunhoffer approximation, the field

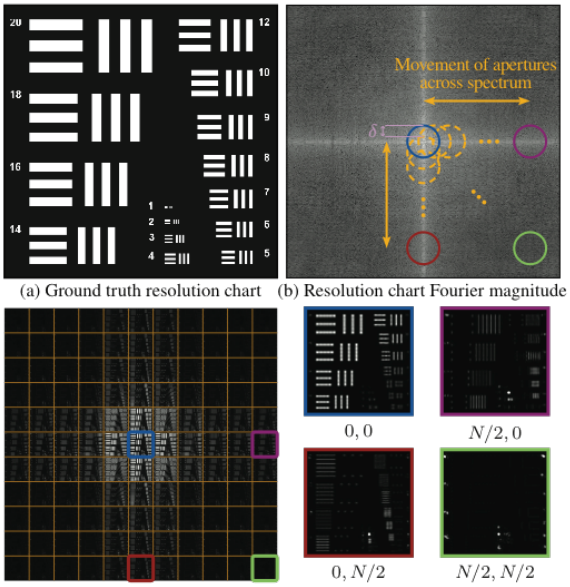


(a) Ground truth resolution chart (b) Resolution chart Fourier magnitude

(c) Observed image mosaic (d) Detail of observed images

**Fig. 2**: Example of image acquisition in Fourier Ptychography. $N \times N$ images with limited, overlapping frequency bands are captured to recover one high resolution image. Image used from [5] with permission.

incident on the lens is a scaled Fourier transform of the scene,

$$\hat{\psi}(u, v) = \mathcal{F}_{\frac{1}{\lambda z}}\left\{\psi(x, y)\right\},$$

where $\lambda$ is the wavelength of illumination, $z$ is the distance between object and lens, $\hat{\psi}(u, v)$ is the field at the lens and $(u, v)$ are coordinates in the frequency domain. The frequency spectrum is limited by the finite aperture of the lens, $A(u - c_u, v - c_v)$, where $(c_u, c_v)$ is the center the lens. The lens focuses the light onto the image plane–which also satisfies the Fraunhofer approximation–and the intensity of the resulting field is recorded by the sensor. The measured intensity is thus given by

$$I(x, y, c_u, c_v) \propto \left|\mathcal{F}\left\{\hat{\psi}(u, v) \odot A(u - c_u, v - c_v)\right\}\right|^2 \quad (1)$$

where $\odot$ signifies an element-wise multiplication. For simplicity, we will drop the the scaling factor of the Fraunhofer approximation in this paper, though it may be accounted for after image reconstruction if desired.

To emulate capturing the scene with a larger lens, $N$ images are captured by translating the lens, $(c_u, c_v)$, to cover a larger portion of the Fourier spectrum. An example of the data acquisition process is shown in Figure 2.

### 2.2. Iterative Error Reduction Algorithm

Recovering the complex field $\hat{\psi}(u, v)$ from the set measured intensity images $I_i$, $i = 1, \ldots, N$, is a non-convex optimization problem. That is, recovering $\hat{\psi}(u, v)$ reduces to solving the optimization problem:

$$\hat{\psi}^* = \text{argmin}_{\hat{\psi}} \sum_i ||\psi_i - \mathcal{F}A_i\hat{\psi}||_2 \quad \text{s.t. } |\psi_i|^2 = I_i,$$

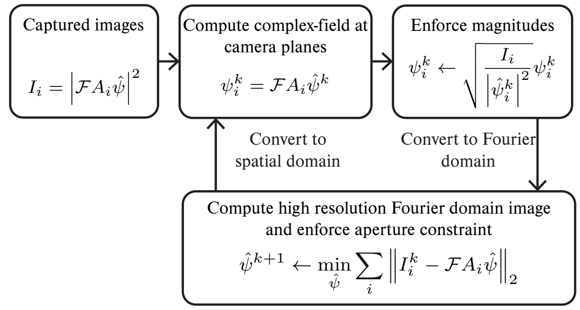


**Fig. 3**: Block diagram for IERA used in [5], modified with permission.

where the spatial arguments have been omitted for compactness. For an ideal lens with radius $r$, light within the support is passed uniformly and all other light is rejected, $A = ||(u - c_u, v - c_v)||_2 \leq r$.

Conventional methods estimate $\hat{\psi}(u, v)$ using variations on iterative error reduction algorithms (IERAs) that enforces magnitude constraints in the spatial domain and support constraints in the Fourier domain [6, 7]. Figure 3 shows the block diagram of the IERA used in [5].

## 3. PTYCHNET

We propose a learning based algorithm of recovering the high resolution image based on Convolutional Neural Networks. An overview of the algorithm is shown in Figure 4 Our network learns a non-linear mapping from the intensity images $I_i$ to the original input light field $\psi$. Both, input $I_i$ and output $\psi$ are in the spatial domain. The inverse filters of the band-passes applied to the original light field can be approximated with convolutional filters and the reconstruction process is locally independent which makes this a well-suited problem for a CNN. The input data of the CNN consists of the concatenation of all the intensity images $I_i$ to a 3D-cube with dimensions $w \times h \times N^2$ where w and h are the width and height of the image and $N^2$ are the number of sampled images. The output of the CNN will directly be the desired high resolution field $\psi$.

### 3.1. Architecture

The proposed CNN is based on the architecture used in [14]. It consists of three convolutional layers. The two hidden layers $H_1$ and $H_2$ are each followed by a ReLU activation function. The first layer has 64 kernels with a kernel size of $9 \times 9$. The second layer has 32 kernels with a size of $5 \times 5$ and the output layer has a kernel size of $5 \times 5$. The output layer has only one kernel that will directly produce the reconstructed image in the spatial domain $\psi$. The weights are initialized with random gaussian distributed values with a standard deviation of 0.001. We use the Euclidean distance as our loss function. Experiments with TV-minimization as loss function did not lead to any improvements in PSNR.

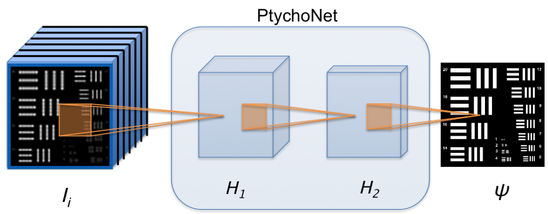


**Fig. 4**: PtychNet Overview

### 3.2. Training Procedure

Our algorithm is implemented with the Caffe framework [18]. We trained our CNN on 91 publicly available images from Set91 [19]. We converted the images to gray-scaled images and resized them to $w \times h$ pixels, where w = h = 512 pixels. These images represent our groundtruth data $\psi$. The forward model from equation 1 was applied to these images to obtain a collection of low quality intensity images $I_i$. The resulting intensity images $I_i$ were resized to $w \times h$ pixels and then concatenated to a 3D-cube of size $w \times h \times N^2$. From these cubes, we extracted about 15,000 patches of size $48 \times 48 \times N^2$ which were used as training database to the CNN. Note that since both the input and the output image of the CNN are in the spatial domain, our reconstruction algorithm is spatially invariant and therefore we can divide the input and output data into patches and process them independently. In order to avoid border effects due to the zero-padding for the convolutional layers, we only use the $32 \times 32$ center pixels of a training patch to calculate the Euclidean loss. We created training datasets of input images with overlapping and non-overlapping frequency bands. For the non-overlapping case, we achieved better performance, if we subtracted the center input image (image at coordinates $0, 0$ in Figure 2) from the reconstructed output image. This approach is similar to the idea of residual networks [13]. Our networks were trained for 200,000 iterations with a batch size of 256.

## 4. EXPERIMENTAL RESULTS

In this section, we tested the effectiveness of our CNN by comparing it against the IERA algorithm proposed in [5]. We tested out algorithm on the commonly used resolution chart (resChart) and lena image. In addition, we used the Set5 images from [19] .We used PSNR and SSIM as our performance metric.The IERA algorithm was evaluated at 100 iterations as the results of IERA did not improve much after 100 iterations. We tested it with the following 2 overlap configurations:

- With 0% Overlap
- With 61% Overlap

where overlap is the percentage of overlap area of the input images in the frequency domain (see Figure 2b). As a baseline, we show the center image (referred to as $Center$) from the input image set (image at position $0, 0$ in Figure 2d), which corresponds to the low pass filtered original image.

### 4.1. Without overlap

Table 1 shows the PSNR and SSIM results for the non-overlapping case. Results are shown for the Center image, IERA and PtychNet. Figure 5 shows the original image and the reconstructed images for the center image, Lena and resChart. We can see that PtychNet produces superior results, both visually as as well as in terms of PSNR/SSIM. Gains from IERA to PtychNet are between 0.6 and 2.1 dBs

### 4.2. With overlap

The IERA and PtychNet images for 61% overlap are shown in Figure 6. Visually, the IERA reconstructed resChart looks more detailed and sharper. The difference in Lena is much less obvious. IERA also outperforms PtychNet in terms of PSNR. Interestingly, the difference of resChart (IERA:18.28, PtychNet:18.04) is much smaller than for Lena (IERA:31.52, PtychNet :29.53). For Set5, the IERA outperforms PtychNet by an average of 2.4dBs (IERA:35.02, PtychNet:32.61).

However PtychNet has a much less runtime than IERA. As a comparison, the runtime for a $512 \times 512$ pixel image for IERA with 100 iterations is about 1 minute, while PtychNet completes in about 0.5 seconds. The IERA algorithm is initialized with the mean image (mean over the 49 input images). Alternatively, we use the output of the PtychNet as initialization image. This leads to a significantly faster convergence of the algorithm, since it is by itself already a good reconstruction of the original image. In Figure 7, we show the average PSNR versus iteration graph for Set5. For comparison, we also initialized the IERA with the center input image, whose bandpass filter is centered around the zero frequency (0,0). While IERA with mean init needs roughly 30 iterations to converge, the PtychNet initialization only requires about 6 iterations to reach the maximum PSNR, which reduces the recovery time by factor 5 and converges to the same PSNR. For the resChart image, the PtychNet initialization even results in a slightly better quality. For all seven test images, the PSNR differs no more than 0.02dBs for the different initialization methods. Hence we can achieve the same performance with IERA, but 5 times faster.

| Image | Metric | Center | IERA | PtychNet |
|---|---|---|---|---|
| lena | PSNR | 25.11 | 24.68 | **25.82** |
| | SSIM | 0.6828 | 0.6488 | **0.7146** |
| resChart | PSNR | 14.41 | 12.92 | **15.05** |
| | SSIM | 0.1981 | 0.1357 | **0.2536** |
| baby | PSNR | 25.97 | 25.46 | **26.50** |
| | SSIM | 0.6836 | 0.6488 | **0.7030** |
| bird | PSNR | 28.49 | 28.50 | **29.70** |
| | SSIM | 0.8175 | 0.8068 | **0.8537** |
| butterfly | PSNR | 21.47 | 21.57 | **23.24** |
| | SSIM | 0.6201 | 0.5866 | **0.7258** |
| head | PSNR | 30.48 | 30.01 | **30.67** |
| | SSIM | 0.7295 | 0.6964 | **0.7410** |
| woman | PSNR | 24.93 | 24.82 | **25.83** |
| | SSIM | 0.7611 | 0.7431 | **0.8106** |

**Table 1**: PSNR and SSIM without overlap

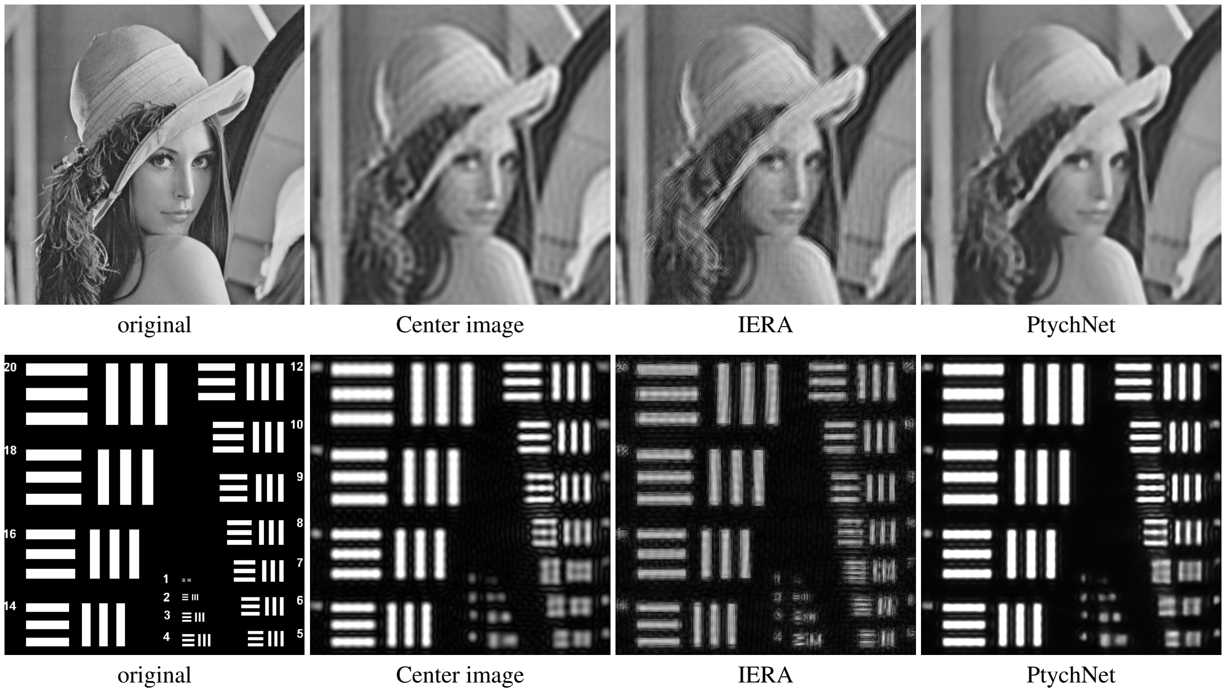


**Fig. 5**: Results with 0% overlap

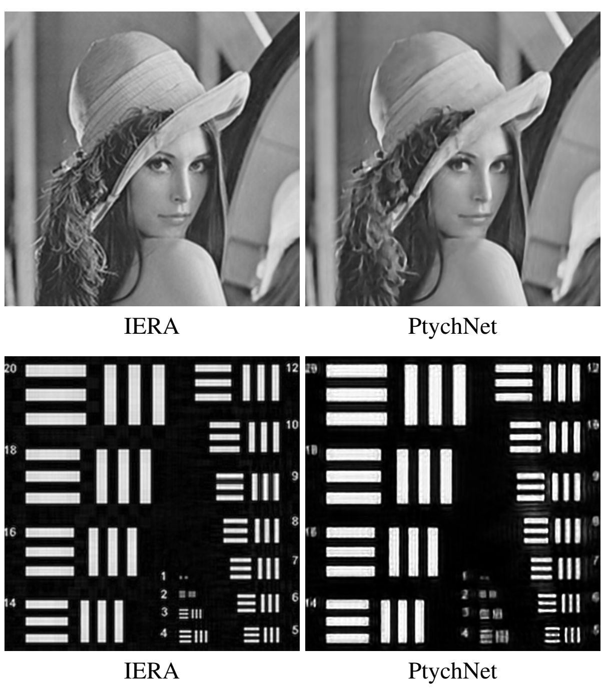


**Fig. 6**: Results with 61% overlap

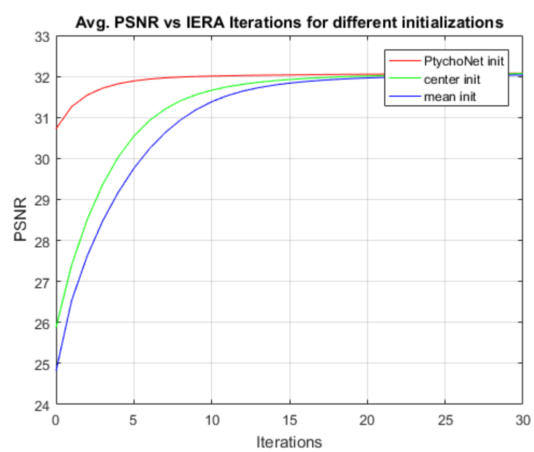


**Fig. 7**: Avg. PSNR over Set5 vs. Iterations for IERA with different initializations. PtychNet initialization shows faster convergence compared to mean and center initializations.

## 5. CONCLUSION

We introduced a recovery algorithm for fourier ptychography based on Deep Learning. To the best of our knowledge, there is no pre-existing work on CNN based fourier ptychography algorithm. We show that in case of non-overlapped fourier sampling, CNNs performed significantly better than the existing IERA algorithm, both, in terms of speed and resolution. Although IERA performs better than PtychNet with overlapping fourier sampling, PtychNet reduces the runtime of the IERA by a factor of 5.

## 6. REFERENCES


[1] Adolf W. Lohmann, Rainer G. Dorsch, David Mendlovic, Carlos Ferreira, and Zeev Zalevsky, "Space–bandwidth product of optical signals and systems," *J. Opt. Soc. Am. A*, vol. 13, no. 3, pp. 470–473, Mar 1996.

[2] Guoan Zheng, Roarke Horstmeyer, and Changhuei Yang, "Wide-field, high-resolution fourier ptychographic microscopy," *Nat Photon*, vol. 7, no. 9, pp. 739–745, Sep 2013, Article.

[3] Xiaoze Ou, Roarke Horstmeyer, Changhuei Yang, and Guoan Zheng, "Quantitative phase imaging via fourier ptychographic microscopy," *Opt. Lett.*, vol. 38, no. 22, pp. 4845–4848, Nov 2013.

[4] Zichao Bian, Siyuan Dong, and Guoan Zheng, "Adaptive system correction for robust fourier ptychographic imaging," *Opt. Express*, vol. 21, no. 26, pp. 32400–32410, Dec 2013.

[5] Jason Holloway, M. Salman Asif, Manoj Kumar Sharma, Nathan Matsuda, Roarke Horstmeyer, Oliver Cossairt, and Ashok Veeraraghavan, "Toward Long Distance, Sub-diffraction Imaging Using Coherent Camera Arrays," *Computational Imaging, IEEE Transactions on*, Submitted for review.

[6] R. W. Gerchberg and W. O. Saxton, "A practical algorithm for the determination of the phase from image and diffraction plane pictures," *Optik (Jena)*, vol. 35, pp. 337, 1972.

[7] J. R. Fienup, "Phase retrieval algorithms: a comparison," *Appl. Opt.*, vol. 21, no. 15, pp. 2758–2769, Aug 1982.

[8] C. Yang, J. Qian, A. Schirotzek, F. Maia, and S. Marchesini, "Iterative Algorithms for Ptychographic Phase Retrieval," *ArXiv e-prints*, May 2011.

[9] Jianliang Qian, Chao Yang, A Schirotzek, F Maia, and S Marchesini, "Efficient algorithms for ptychographic phase retrieval," *Inverse Problems and Applications, Contemp. Math*, vol. 615, pp. 261–280, 2014.

[10] Pavel Sidorenko and Oren Cohen, "Single-shot ptychography," *Optica*, vol. 3, no. 1, pp. 9–14, Jan 2016.

[11] Alex Krizhevsky, Ilya Sutskever, and Geoffrey E Hinton, "Imagenet classification with deep convolutional neural networks," in *Advances in Neural Information Processing Systems 25*, F. Pereira, C. J. C. Burges, L. Bottou, and K. Q. Weinberger, Eds., pp. 1097–1105. Curran Associates, Inc., 2012.

[12] Christian Szegedy, Wei Liu, Yangqing Jia, Pierre Sermanet, Scott Reed, Dragomir Anguelov, Dumitru Erhan, Vincent Vanhoucke, and Andrew Rabinovich, "Going deeper with convolutions," in *Proceedings of the IEEE Conference on Computer Vision and Pattern Recognition*, 2015, pp. 1–9.

[13] Kaiming He, Xiangyu Zhang, Shaoqing Ren, and Jian Sun, "Deep residual learning for image recognition," in *Proceedings of the IEEE Conference on Computer Vision and Pattern Recognition*, 2016, pp. 770–778.

[14] Armin Kappeler, Seunghwan Yoo, Qiqin Dai, and Aggelos K Katsaggelos, "Video super-resolution with convolutional neural networks," *IEEE Transactions on Computational Imaging*, vol. 2, no. 2, pp. 109–122, 2016.

[15] C. Dong, C. C. Loy, K. He, and X. Tang, "Image super-resolution using deep convolutional networks," *IEEE Transactions on Pattern Analysis and Machine Intelligence*, vol. 38, no. 2, pp. 295–307, Feb 2016.

[16] Christian Ledig, Lucas Theis, Ferenc Huszár, Jose Caballero, Andrew Cunningham, Alejandro Acosta, Andrew Aitken, Alykhan Tejani, Johannes Totz, Zehan Wang, et al., "Photo-realistic single image super-resolution using a generative adversarial network," *arXiv preprint arXiv:1609.04802*, 2016.

[17] Jonathan Long, Evan Shelhamer, and Trevor Darrell, "Fully convolutional networks for semantic segmentation," in *Proceedings of the IEEE Conference on Computer Vision and Pattern Recognition*, 2015, pp. 3431–3440.

[18] Yangqing Jia, Evan Shelhamer, Jeff Donahue, Sergey Karayev, Jonathan Long, Ross Girshick, Sergio Guadarrama, and Trevor Darrell, "Caffe: Convolutional architecture for fast feature embedding," in *Proceedings of the 22nd ACM international conference on Multimedia*. ACM, 2014, pp. 675–678.

[19] J. Yang, J. Wright, T. S. Huang, and Y. Ma, "Image super-resolution via sparse representation," *IEEE Transactions on Image Processing*, vol. 19, no. 11, pp. 2861–2873, Nov 2010.